GEOPHYSICS, VOL. 75, NO. 3 (MAY-JUNE 2010); P. B103–B114, 9 FIGS.
10.1190/1.3377009

Case History

Unexploded ordnance discrimination using magnetic and electromagnetic sensors: Case study from a former military site

Stephen D. Billings[1], Leonard R. Pasion[2], Laurens Beran[3], Nicolas Lhomme[1], Lin-Ping Song[3], Douglas W. Oldenburg[3], Kevin Kingdon[1], David Sinex[3], and Jon Jacobson[1]

ABSTRACT

In a study at a military range with the objective to discriminate potentially hazardous 4.2-inch mortars from nonhazardous shrapnel, range, and cultural debris, six different discrimination techniques were tested using data from an array of magnetometers, a time-domain electromagnetic induction (EMI) cart, an array of time-domain sensors, and a time-domain EMI cart with a wider measurement bandwidth. Discrimination was achieved using rule-based or statistical classification of feature vectors extracted from dipole or polarization tensor models fit to detected anomalies. For magnetics, the ranking by moment yielded better discrimination results than that of apparent remanence from relatively large remanent magnetizations of several of the seeded items. The magnetometer results produced very accurate depths and fewer failed fits attributable to noisy data or model insufficiency. The EMI-based methods were more effective than the magnetometer for intrinsic discrimination ability. The higher signal-to-noise ratio, denser coverage, and more precise positioning of the EM-array data resulted in fewer false positives than the EMI cart. When depth constraints from the magnetometer data were used to constrain the EMI fits through cooperative inversion, discrimination performance improved considerably. The wide-band EMI sensor was deployed in a cued-interrogation mode over a subset of anomalies. This produced the highest-quality data because of collecting the densest data around each target and the additional late time-decay information available with the wide-band sensor. When the depth from the magnetometer was used as a constraint in the cooperative inversion process, all 4.2-inch mortars were recovered before any false positives were encountered.

INTRODUCTION

Unexploded ordnance (UXO) poses a major safety hazard in many parts of the world, including Canada, the United States, and Australia, where UXO is present at former and active military ranges. During the past 10 years, significant research effort has been focused on developing methods to discriminate between hazardous UXO and nonhazardous scrap metal, shrapnel, and geology (e.g., Bell et al., 2001; Collins et al., 2001; Hart et al., 2001; Pasion and Oldenburg, 2001; Zhang et al., 2003a; Zhang et al., 2003b; Billings, 2004). The most promising discrimination methods typically proceed by first recovering a set of parameters that specify a physics-based model of the object being interrogated. For example, in time-domain electromagnetic (TEM) data, the parameters are the object location and the polarization tensor (typically two or three collocated orthogonal dipoles along with their orientation and some parameterization of the time-decay curve). For magnetics, the physics-based model is generally a static magnetic dipole. Once the parameters are recovered by inversion, a subset of the parameters is used as feature vectors to guide a statistical or rule-based classifier. There are significant advantages in collecting both types of data, including increased detection, stabilization of EM inversions by cooperative inversion of the magnetics (Pasion et al., 2008), and extra dimensionality in the feature space that may improve classification performance (e.g., Zhang et al., 2003a).

Manuscript received by the Editor 25 June 2009; revised manuscript received 16 September 2009; published online 20 May 2010.
[1]Sky Research Inc., Vancouver, British Columbia, Canada. E-mail: stephen.billings@skyresearch.com; nicholas.lhomme@skyresearch.com; kevin.kingdon@skyresearch.com; jon.jacobson@skyresearch.com.
[2]Sky Research Inc., Vancouver, British Columbia, Canada, and The University of British Columbia, Geophysical Inversion Facility, Vancouver, British Columbia, Canada. E-mail: leonard.pasion@skyresearch.com.
[3]The University of British Columbia — Geophysical Inversion Facility, Vancouver, British Columbia, Canada. E-mail: lberan@eos.ubc.ca; lpsong@eos.ubc.ca; doug@eos.ubc.ca; dsinex@eos.ubc.ca.

Results are presented here for a discrimination study pilot program conducted at the former Camp Sibert, Alabama, U.S.A., sponsored by the Environmental Security Technology Certification Program (ESTCP). The ability to separate munitions from nonhazardous metallic items or geology is critical to reduce the cost of remediating munitions-contaminated sites. Camp Sibert is particularly well suited for such classification efforts, which require collecting high-quality geophysical data. The site is relatively flat and clear of obstructions from vegetation or topography that would hinder surveying with cart-based geophysical sensors. In addition, the history of the site indicates there was primarily one type of ordnance deployed there: 4.2-in mortars. The objective at Camp Sibert was to discriminate potentially hazardous 4.2-inch mortars from nonhazardous shrapnel, range, and cultural debris.

Our case study focuses on the results achieved using methodologies developed by ourselves and others (e.g., Pasion and Oldenburg, 2001; Billings, 2004; Beran and Oldenburg, 2008; Pasion et al., 2008). We provide an overview of the methodology and point the reader to relevant papers that describe the techniques in greater detail. We concentrate primarily on the results achieved — in particular, the comparative performance of the different sensor modalities and deployment modes. All results reported here were obtained using commercial off-the-shelf (COTS) sensors. These include Geonics EM61 and EM63 time-domain metal detectors and an array of Geometrics cesium vapor magnetometers. See Gasperikova et al. (2009) for the results of applying a multistatic EMI sensor at the same site.

Because each COTS instrument measures only one component of a vector field, a measurement at a single location provides limited information. Consequently, relatively dense 2D measurements are required for accurate recovery of relevant target parameters. These measurements must be very precisely positioned and oriented for discrimination to be successful. Data were acquired in full-coverage survey mode (magnetometer array, EM61 cart, and EM61 array) and in cued-interrogation mode (EM63 cart), whereby selected prelocated anomalies were surveyed densely in the immediate vicinity of the flagged anomaly location picked from a full coverage survey. In addition to inverting each of the individual sets of data discussed, cooperative inversions also were undertaken for the towed EM61 array and the EM63 cued-mode data using the magnetometer data to constrain the EM inversions.

Here, we contrast the discrimination and localization abilities of six sensor combinations:

1) Magnetometer array deployed in full-coverage mode with dipole moment size used for discrimination
2) EM61 cart deployed in full-coverage mode (no orientation information recorded)
3) EM61 array deployed in full-coverage mode with position and orientation information recorded
4) Cooperative inversion of EM61 array and magnetometer array data
5) EM63 cart deployed in cued-interrogation mode with position and orientation recorded
6) Cooperative inversion of EM63 cart and magnetometer array data

STRUCTURE OF DISCRIMINATION STUDY

Our results are from a blind test of the discrimination performance of the different techniques; the ESTCP managed the discrimination study and withheld ground-truth information until after discrimination declarations had been made. All results reported here, unless otherwise indicated, were for the original submissions to the ESTCP.

An initial magnetometer survey of the Camp Sibert site was used to select three different areas for the discrimination study: southeast 1 (SE1), southeast 2 (SE2), and southwest (SW). Combined, the three areas cover approximately 15 acres. A geophysical prove-out (GPO) was established immediately adjacent to the SW area; it included 30 4.2-inch mortars emplaced at different depths and orientations and eight partial mortars, considered as nonhazardous scrap. The ESTCP emplaced 152 4.2-inch mortars in the three areas. The locations and depths of 29 of these mortars, along with the locations and identities of 179 clutter items, were provided to each demonstrator and used as training data.

In full-coverage survey mode, data were collected using the standard cart platform of the EM61-MK2 system. The Geonics EM61-MK2 is a pulse-based time-domain electromagnetic instrument that records data in four time windows centered at 0.216, 0.366, 0.660, and 1.266 ms after pulse turn-off (e.g., Bosnar, 2001). EM61-MK2 cart data were acquired by an onsite contractor using a line spacing of 50 cm, sensor height of 40 cm, and positions recorded with a real-time kinematic global position system (RTK GPS), accurate to within a few centimeters. Survey-mode data also were acquired for a magnetometer array and an EM61-MK2 array using the multisensor towed-array detection system (MTADS). The MTADS EM array consists of three overlapping EM61-MK2 sensors (each 1 m wide and 0.5 m long) that have a center-to-center separation of 0.5 m (Nelson et al., 2003). Data were collected with a nominal across-track sensor spacing of 50 cm, and the array was transported 25 cm above the ground.

Figure 1 shows the MTADS EM data over the SW area with the location and identities of the ground truth marked. The MTADS magnetometer array is composed of a platform housing a 2-m-wide inline array of eight G-822 cesium vapor magnetometers spaced 25 cm apart and 25 cm above the ground (Nelson et al., 2003). For the MTADS EM and magnetometer arrays, position and orientation information were obtained through centimeter-level RTK GPS and inertial-motion-unit (IMU) measurements.

The Geonics EM63 is a pulse-based multichannel TEM induction instrument (e.g., McNeil and Bosnar, 2000). The system consists of a 1×1-m-square transmitter coil and three coaxial 0.5×0.5-m-square receiver loops mounted on a two-wheeled trailer. Measured voltages are averaged over 26 geometrically spaced time gates, spanning 180 μs to 25.14 ms. The EM63 was deployed in a cued-interrogation mode on a customized air-suspension cart. The cart lowered the instrument closer to the surface (from the standard 40 cm to 20 cm) and absorbed some of the effects from instrument jostle resulting from an uneven ground surface. The late-time information available from the 26 time channels provided an extended view of target decays. Position information was collected by a Leica TPS 1206 robotic total station with orientation effects recorded using a Crossbow AHRS 400 IMU. We estimated that positions were accurate to within 2–4 cm and orientation to within about 2°.

DATA PROCESSING AND INTERPRETATION METHODOLOGY

Three steps are required to utilize geophysical data for unexploded ordnance discrimination. First, we create a map of the geophysical sensor data; this includes all actions required to estimate the geophysical quantity in question (magnetic field, amplitude of EMI response at a given time channel, etc.) at each visited location. Second, we select the anomaly and extract features. This includes detecting anomalous regions and subsequently extracting a dipole (magnetics) or polarization tensor model (TEM) for each anomaly. Where magnetic and EMI data have been collected, the magnetic data are used as constraints for the EMI model via a cooperative inversion process. Third, we classify anomalies. The objective of the demonstration is to produce a dig sheet with a ranked list of anomalies. We achieve this using statistical classification, which requires training data to determine the attributes of the UXO and non-UXO classes.

Process flow

Each demonstrator provided filtered, located geophysical data. No additional preprocessing was performed on any data set. At this point in the process flow, there was a map of each of the geophysical quantities measured during the survey. The next step in the process was to detect anomalous regions, followed by extracting features for each detected item. Anomalous regions were detected by the demonstrators who provided the easting and northing coordinates corresponding to the maximum geophysical signature for each anomaly. The demonstrators used an automatic target-detection algorithm that triggered a detection each time the sensor response exceeded a threshold. The threshold value was set to one-half of the minimum amplitude recorded over any of the 4.2-inch mortars in the GPO.

The inversion procedure assumes that we are dealing with a single target in free space. Once data anomalies are identified, we define a mask to represent the spatial limits of the data to be inverted. Unlike magnetics data, an unconstrained EMI inversion is very sensitive to adjacent anomalies and to the size of the mask used in areas without nearby anomalies. The masking procedure helps ensure that signals from adjacent anomalies do not affect the inversion results. In addition, from a practical standpoint, inverting the minimum number of observations reduces computing time.

We used an automated masking procedure that fits an ellipse to contours of the anomalous target. By using an ellipse, we recover a relatively smooth mask that mimics the shape of the anomaly. The main challenge is to find contours that are smooth as well as close to the noise level. Including good estimates of the background noise ensures that we choose appropriate starting contour values that are above the baseline error and encompass all anomalous data. Estimates of background noise were calculated independently for each time channel through the statistics in a 5×5 -m moving window that covered the entire data set. To estimate the standard deviation of the noise, the sample skewness was calculated and the largest data samples were iteratively discarded until the skewness value was less than a user-defined threshold value (we used 0.25). This process provided an effective means to estimate the spatially (and temporally) varying background noise without significant distortion from the signals of interest.

We did not always include all time channels in the inversion process. For the EM61, we kept, at a minimum, the first three time channels; for the EM63, we kept, at a minimum, the first 10 time channels. Additional channels were included if the energy within the mask at that time channel were at least twice the estimated noise level.

Feature extraction for a magnetics sensor

For magnetics, the physics-based model most commonly used is a dipole:

$$\mathbf{b}(\mathbf{r}) = \frac{\mu_0}{4\pi r^3}((\mathbf{m}\cdot\hat{\mathbf{r}})\hat{\mathbf{r}} - \mathbf{m}), \tag{1}$$

where $\hat{\mathbf{r}} = \mathbf{r}/|\mathbf{r}|$ is the unit vector pointing from the dipole to the observation point, $\mathbf{b}$ is the vector magnetic field, $\mathbf{m}$ is a magnetic dipole, $\mu_0 = 4\pi \times 10^{-7}$ H/m is the permittivity of free space, and $r = |\mathbf{r}|$ is the distance between the center of the object and the observation point. A bound-constrained optimization problem is solved to extract feature vectors from each anomaly (Branch et al., 1999).

The magnetic remanence metric was calculated for each dipole moment (Billings, 2004) by using an equivalent spheroid to represent a 4.2-inch mortar. The equivalent spheroid defines a dipole feasibility curve (the family of moments that an object of that length and

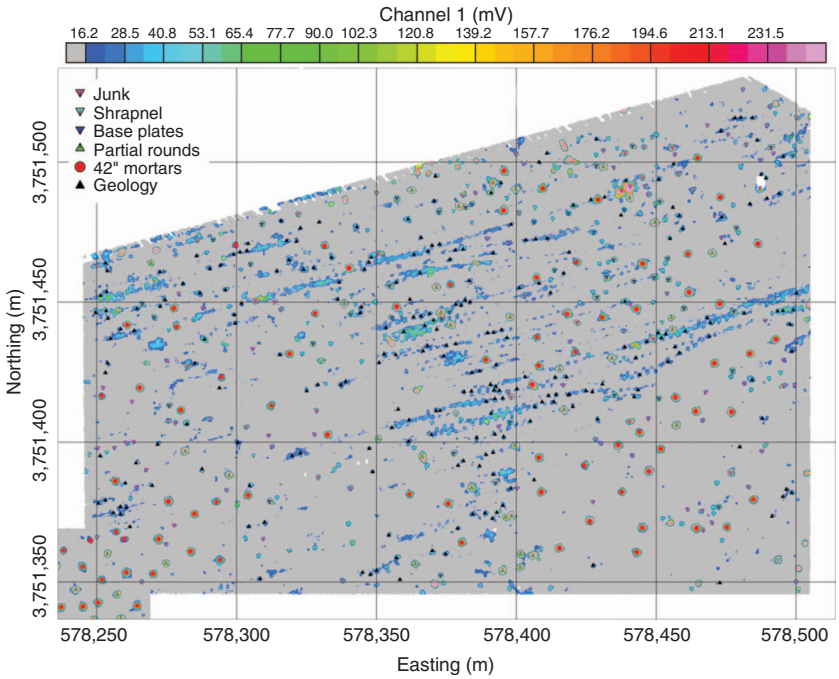

Figure 1. MTADS-EM61 map of the southwest area of the former Camp Sibert. Note the artifacts caused by cart bounce as the MTADS-EM61 array traversed perpendicular furrows in a recently plowed field.

diameter can produce by induced magnetization in the presence of the earth's magnetic field). We calculated the orientation that causes the minimum difference $\Delta\mathbf{m}$ between the moment of the ordnance and the moment determined through the inversion $\mathbf{m}$. We then estimated the minimum percentage of remanent magnetization required to best match the observed dipole:

$$\text{rem} = 100\frac{\|\Delta\mathbf{m}\|}{\|\mathbf{m}\|}. \tag{2}$$

Feature extraction for a time-domain EMI sensor

In general, TEM sensors use a step-off field to illuminate a buried target. The currents induced in the buried target decay with time, generating a decaying secondary field that is measured at the surface. The time-varying secondary magnetic field $\mathbf{b}(t)$ at a location $\mathbf{r}$ from the dipole $\mathbf{m}(t)$ can be approximated with a dipole as per equation 1 except, in this case, the moment is a function of time. The dipole induced by the interaction of the primary field $\mathbf{b}_0$ and the buried target is given by

$$\mathbf{m}(t) = \frac{1}{\mu_0}\mathbf{M}(t)\cdot b_0, \tag{3}$$

where $\mathbf{M}(t)$ is the target's polarization tensor (e.g., Das et al., 1990; Bell et al., 2001; Pasion and Oldenburg, 2001; Smith et al., 2004).

The polarization tensor governs the decay characteristics of the buried target and is a function of the shape, size, and material properties of the target. The polarization tensor is written as

$$\mathbf{M}(t) = \begin{bmatrix} L_1(t) & 0 & 0 \\ 0 & L_2(t) & 0 \\ 0 & 0 & L_3(t) \end{bmatrix}, \tag{4}$$

where we use the convention that $L_1(t_1) \geq L_2(t_1) \geq L_3(t_1)$, so that polarization-tensor parameters are organized from largest to smallest. The polarization-tensor components are parameterized such that the target response can be written as a function of a model vector containing components that are a function of target characteristics. Particular parameterizations differ, depending on the instrument (number of time channels, time range measured, etc.) and the group implementing the work. Bell et al. (2001) solve for the components of the polarization tensor at each time channel, and this is the procedure we use for the four-channel EM61-MK2. For the EM63, we use the Pasion-Oldenburg (2001) formulation:

$$L_i(t) = k_i(t + \alpha_i)^{-\beta_i}\exp^{-t/\gamma_i} \tag{5}$$

for $i = \{1,2,3\}$, with the convention that $k_1 \geq k_2 \geq k_3$. For a body of revolution, $L_2 = L_3$ for a rodlike object (Pasion and Oldenburg, 2001) and $L_1 = L_2$ for a platelike object.

A bound-constrained optimization problem is solved for the three polarization tensor components, their three Euler angles, and the three position coordinates of the source (Branch et al., 1999; Billings et al., 2002).

Feature extraction for cooperative inversion of TEM and magnetic data

In cooperative inversion, multiple data are inverted sequentially; the results of the first inversion constrain the second (Pasion et al., 2008). This prior information can be introduced formally into the Bayesian formulation through the prior $p(\mathbf{v})$, where $\mathbf{v}$ is a vector of model parameters. Commonly utilized priors include Gaussian and uniform priors (i.e., a constant probability density function [PDF] for a parameter between two limits and zero probability outside these limits). The solution to the inverse problem, given observed data $\mathbf{d}^{\text{obs}}$, utilizes a Gaussian prior with hard bounds:

$$\text{minimize } \phi(\mathbf{v}) = \sum_j \frac{1}{2\sigma_j^2}(v_j - \bar{v}_j)^2 + \frac{1}{2}\|\mathbf{V}_d^{-1/2}(\mathbf{d}^{\text{obs}} - \mathbf{F}(\mathbf{v}))\|^2, \quad \text{subject to } v_i^L \leq v_i \leq v_i^U, \tag{6}$$

where j represents the index of parameters distributed as Gaussian PDFs with standard deviation σ_j, $\mathbf{V}_d^{-1/2}$ is the inverse square root of the data covariance matrix, and $\mathbf{F}(\mathbf{v})$ is the forward model operation (returns predicted data given the model parameters $\mathbf{v}$).

We used a three-step strategy for cooperatively inverting magnetics and electromagnetics data. First, the magnetics data were inverted for a best-fit dipole. Second, the dipole location was used to define $\bar{v}_j$ (for $j = 1$, 2, and 3 that correspond to the easting, northing, and depth of the dipole) and the standard deviation of the parameter uncertainties used to define σ_j. The estimated model-parameter standard deviations were obtained from the Gauss-Newton approximation to the Hessian at the optimum model location (e.g., Billings et al., 2002). Third, we inverted the EM data using the prior obtained from the magnetics data in step 2.

Inevitably, there were anomalies in the TEM data that did not have corresponding magnetic fits, and vice versa. Where no constraints from magnetometer data were available, the TEM data were inverted using the same procedure as for single inversion.

Data-quality considerations using a figure of merit (FOM)

In all data sets, there are a number of targets whose observed fit obtained through the inversion process is unsatisfactory and must be failed. These failed fits were classified as "can't analyze" and would have resulted in a significant number of excavations. We therefore investigated methods to reduce the number of items that needed to be excavated, hoping to maintain the same probability of correct classification.

Close scrutiny of failed inversions and inversions that yielded inaccurate depth estimates on the GPO and ground-truth targets revealed that poor inversions could be tied to certain features of the data or the inversion. This motivated us to identify and establish rules to define a confidence factor for a given inversion. We considered several criteria that we gathered under a so-called figure of merit (FOM), which comprises the following data features:

- Signal-to-noise ratio (S/N) should be above a given threshold for reliable inversion of each time channel; S/N should decay with time if the sensor operates properly and noise estimates are accurate.
- Data coverage of anomaly should sample the spatial decay of the

EM scattered field to allow recovery of orthogonal polarizations.

The data inversion features include the following:

- Quality of fit — misfit, correlation coefficient.
- Variance of estimated depth — there can be several solutions of the inverse problem with similar misfits but distributed over a large range of depth.

Full details and quantitative descriptions of each FOM metric are provided in Lhomme et al. (2008).

Discrimination methodology

For the magnetic data, the primary discrimination diagnostic was based on the size of the dipole moment (with a preference to dig items with larger moments). For test purposes, we compiled a second discrimination ranking using the apparent magnetic remanence (equation 2). Data from the GPO and the initial release of training data were used to determine appropriate thresholds for dipole size and remanence. The dipole-size threshold was selected based on the minimum moment of a 4.2-inch mortar encountered in the GPO and training data, with an extra safety margin built in to account for error in estimating the depth of the dipole (which could cause an underestimate of the size of the moment). The remanence threshold was set at 10% larger than the maximum apparent remanence encountered in the GPO and training data.

For the statistical classification, we used data over the GPO and the initial training grids to determine which feature vectors and statistical classifier to use. A probabilistic neural network (PNN) was trained on a size and a time-decay feature extracted from anomalies in the GPO (thirty 4.2-inch mortars and eight cutter items) and the partial release of ground truth (29 mortars and 179 clutter items). The PNN classifier models the underlying statistical distributions as a superposition of Gaussian kernel functions centered on each training vector, with the kernel width set to the standard deviation of the feature vectors in the UXO class. The size feature was chosen as the base-10 logarithm of the maximum instantaneous polarization at time channel 1 for the EM61 and the base-10 logarithm of the largest Pasion-Oldenburg k-parameter for the EM63. Relative time decays were calculated as the ratio of the principal polarizations of the third and first time channels for the EM61 and as the ratio of the principal polarizations at the fifteenth and first time channels for the EM63. The size and time-decay features were then normalized so they had zero mean and unit variance. Stop-digging points were selected by visually inspecting the training data and the PNN probability surface.

From the extracted feature vectors, the following five statistically based dig sheets were produced:

1) MTADS-EM61, using statistical classification of features derived from the MTADS-EM61 data
2) Contractor EM61, using statistical classification of features derived from the Contractor's EM61 data
3) EM63 cued, using statistical classification of features derived from the EM63 cued-interrogation data
4) MTADS-EM61 and magnetics as for dig sheet 1 but with MTADS-EM61 fits constrained by the magnetics data and adding features from the magnetometer data (remanence, moment, etc.)
5) EM63 and magnetics as for dig sheet 4 but with the EM63.

RESULTS FROM CAMP SIBERT

Survey-mode data

Figure 2 plots the two feature vectors for the MTADS magnetics, EM61 cart, MTADS-EM61, and MTADS-EM61 cooperative data sets over the decision surface, with separate plots for the training and test data. For magnetics, the training data revealed several 4.2-inch mortars with relatively large remanence (Figure 2a). All mortars had moments greater than 0.17 Am^2 and could therefore be considered large. Consequently, the size of the moment (not the remanence) was used to prioritize the dig list. We also produced a remanence prioritized dig list so that we could test performance using that discrimination metric. Assuming a 5-cm error in the depth estimate of the dipole moment at the surface, we anticipated that all mortars would be recovered with a threshold of 0.109 Am^2, which we decreased to 0.1 Am^2 for an extra safety margin. In other words, we recommended digging all anomalies with moments greater than 0.1 Am^2.

Feature vectors within the UXO, partial rounds, and base-plate classes are more tightly clustered for the MTADS-EM61 than for the EM61 cart, with further improvement evident in the cooperatively inverted MTADS-EM61. This indicates higher-quality data obtained using the MTADS-EM61 array, which has the additional capability over the EM61 cart of recording sensor orientation by incorporating IMU and collecting orthogonal sets of survey lines. Further improvements are obtained when the EM61-MTADS is cooperatively inverted because incorporating the MTADS magnetometer measurements considerably improves the accuracy of the estimated depths. For all three data sets in Figure 2, we used two decision boundaries: an aggressive one for high FOM anomalies and a less aggressive one for low FOM anomalies. For each of the three data sets, all 4.2-inch mortars lay on the appropriate side of the "high-confidence UXO" decision boundary.

Figure 3 compares the magnetometer, EM61, MTADS-EM61, and MTADS-EM61 cooperative receiver operating characteristic (ROC) curves. The horizontal axis shows the number of unnecessary excavations required (items that had to be dug but were not 4.2-inch mortars) with the vertical axis, showing the proportion of mortars in the test set that were recovered. A solid dot represents the operating point (i.e., the stop-digging point) of each classification method. Some anomalies had insufficient S/N or data coverage to constrain the TEM model parameters. This included anomalies with overlapping signatures that could not be isolated and inverted one at a time. All such anomalies were labeled "can't analyze" on the dig sheet and excavated as potential UXO. When including the "can't analyze" category (Figure 3a), the magnetometer data require the fewest number of false-positive (FP) excavations at its operating point (170 compared to 264, 344, and 275 for the EM61, MTADS-EM61, and MTADS-EM61 cooperative). For the non-UXO items, 72% can be left in the ground with the magnetometer data, compared to 33%, 44%, and 55% for the other data sets. When excluding the "can't analyze" category (Figure 3b), it is evident that feature vectors extracted from the MTADS-EM61 and MTADS-EM61 cooperatively inverted data are more highly discriminatory than the magnetometer or EM61.

Addressing the problem of the large number of "can't analyze" anomalies

The MTADS-EM61 and MTADS-EM61 cooperative algorithms had to deal with many geologic detections that could not be fit by the

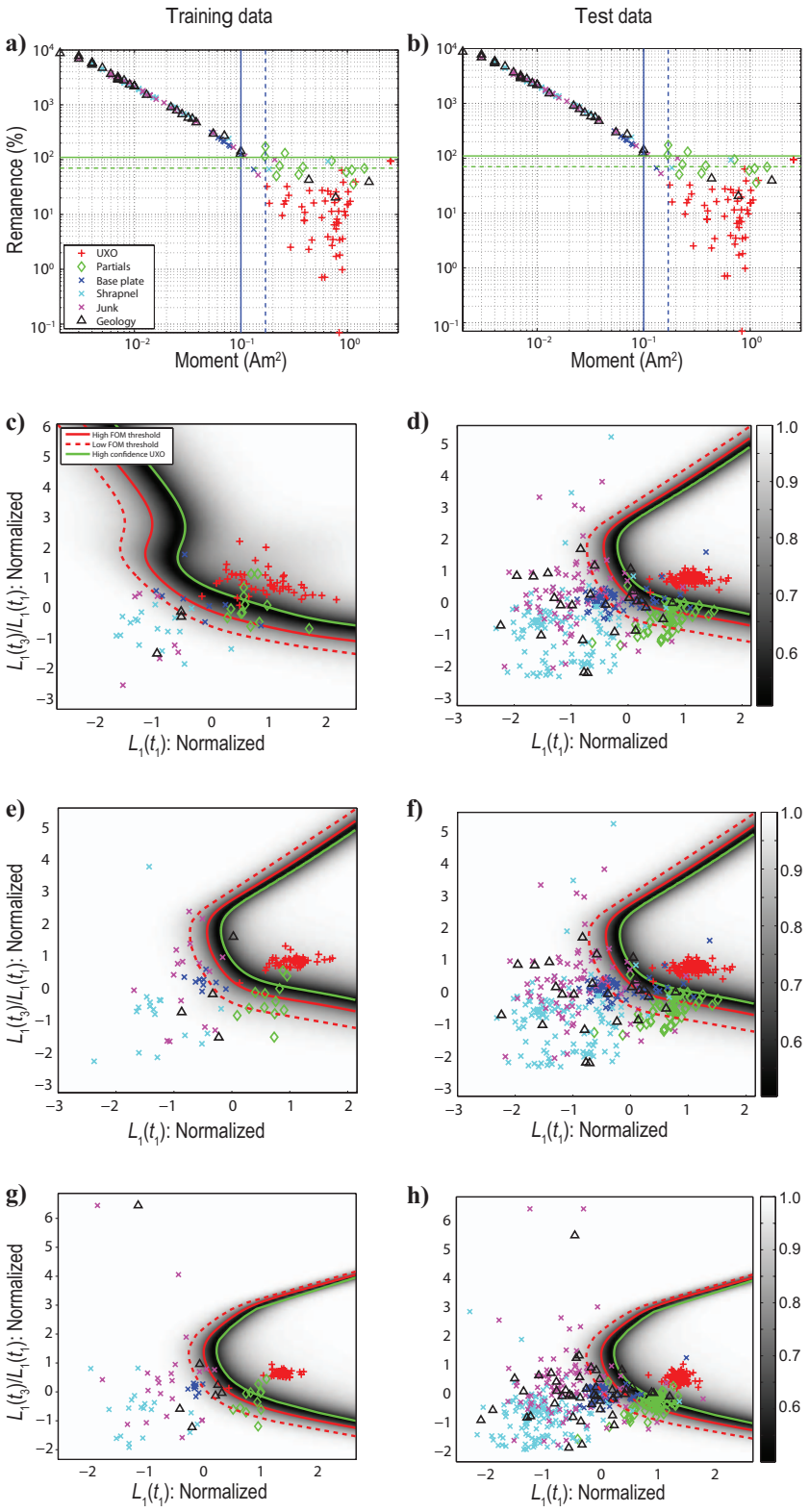

Figure 2. Scatter plot of moment versus remanence for training data (left column) and test data (right column). (a, b) MTADS magnetometer. Vector plots for (c, d) contractor EM61, (e, f) MTADS-EM61, and (g, h) MTADS-EM61 cooperative data sets. The PNN classifier probability is shown as a grayscale image. Black represents feature vectors with equal probability of being in either class. The color scale grades to white for the UXO and non-UXO classes. For the magnetics methods, stop-digging thresholds are delineated by dashed lines (blue for moment, green for remanence), with the minimum values encountered in the training data delineated by solid lines.

dipole model and hence had to be listed as "can't analyze." These extra false detections caused the MTADS classifiers to have poorer performance than the magnetometer and EM61 cart when "can't analyze" anomalies were included. Most of these geologic alarms were caused by the bouncing movement of the cart as it traversed furrows in the plowed field on the southwest section of the site. When the distance between the cart and the ground decreased, there was an increase in the amplitude of the response from the soil, which often was large enough to trigger a false detection. A scatter plot of the total energy of time channel t_1 of the east-west versus north-south transects (Figure 4a) shows that most of the geologic anomalies have 18–23 dB of energy north-south (perpendicular to furrows) compared to 5–18 dB east-west (parallel to furrows).

To reduce the number of geological anomalies, we decided to try to develop a metal/soil discriminator based on the relative energy in the two directions. This was to be applied as a prescreener before submitting the anomaly to the polarization tensor-fitting routines. We used the GPO and initial training data to investigate different potential classifiers and used two classes: one comprising the geologic anomalies and the other comprising all metallic anomalies minus fragmentation (the S/N of anomalies resulting from fragmentation was generally very low, and there often were significant differences between the north-south and east-west transects). After initial experimentation, we settled on a quadratic discriminant analysis classifier because it produced the most intuitively reasonable discrimination boundary. We then plotted the cumulative distributions of the different classes against the metal probability P_{metal} (Figure 4c). Approximately 50% of geologic anomalies had $P_{\text{metal}} < 0.3$, with the first UXO occurring at $P_{\text{metal}} = 0.4$. We therefore selected an operating point of $P_{\text{metal}} < 0.3$.

Figure 4b shows a feature vector plot of the blind-test data, and Figure 4d shows cumulative distributions of the different classes. At the selected operating point, 55% of geologic anomalies would be rejected, along with 14% of shrapnel, 8% of scrap metal, and less than 3% of partial rounds and base plates. Most importantly, no UXO would be rejected by the prescreener. It would have excluded 119 geologic anomalies from further analysis: 116 of these were in the "can't analyze" category and had to be excavated. In total, the prescreener could have reduced the number of "can't analyze" anomalies by 130 (from 285 to 155). For the MTADS-EM61 cooperative inversion, the reduction would have dropped from 226 to 116.

Note that this prescreener was applied retrospectively and was not used for the initial submission of dig sheets.

Cued-interrogation-mode data

The EM63 was deployed in a cued-interrogation mode over a subset of anomalies; the blind-test data comprised 150 items that contained 34 UXO. Statistical classification results are presented for EM63 data and EM63 cooperatively inverted data in Figures 5 and 6. As with the EM61 data sets, discrimination was based on a PNN classifier with a size-based and a time-based feature vector. The size-based feature vector was the k_1-parameter from the primary polarization, with the ratio of primary polarizations at the fifteenth and first time channels used as the time-decay parameter. The UXO, partial rounds, and base-plate classes are tightly clustered in both data sets, with fewer variation in the cued-interrogation data (Figure 5). The UXO class for the EM63 data contain two outliers, one of which causes the false negative evident in Figure 5b. At the selected operating point, the EM63 statistical classification required 38 false positives (30 of these were "can't analyze"), but one 4.2-inch mortar was missed.

The EM63 false negative was from a 4.2-inch mortar buried at 40 cm that was predicted to be at 5 cm. The shallower solution depth underestimated the size of the item and resulted in the feature vector lying outside the main cluster of the 4.2-inch mortar class. Inspection of the observed data and model fit reveals a very poor fit to one of the transverse lines in the cued-interrogation data (Figure 7). This line of bad data should have been identified and removed so that the false negative would have been a consequence of a quality-control (QC) failure. A misfit versus depth plot (Figure 8) reveals two minima: one at the shallow solution and another close to the true depth of 40 cm. The shallower solution has a slightly lower misfit and hence is selected by the optimization algorithm. After removing the corrupt line of data, the misfit of the shallow solution increases and the deeper solution is preferred (Figure 8). A better size estimate results, and the feature vector for the anomaly lies within the same tight cluster as the rest of the mortars. When the depth constraints from the magnetometer were used, the deeper solution was also preferred and the false negative was eliminated. This example demonstrates the importance of careful QC and the benefits of the cooperative inversion procedure. Even a simple automated QC process that flags residuals above a certain threshold would have identified this anomaly.

When the depth from the magnetometer was used as a constraint in the cooperative inversion process, the false negative did not occur. In fact, the EM63 cooperative produced a perfect ROC curve, with all 34 UXO recovered and zero false alarms. At the selected operating point, 21 false positives were required, with 16 of these in the "can't analyze" category. In Figure 6, we also show an ROC curve for the MTADS-EM61 cooperative when restricted to the same 150 cued-interrogation anomalies. It results in a perfect ROC curve but requires 34 FP at the operating point, with six of those in the "can't analyze" category.

Accuracy of inverted depths

Scatter plots of the predicted versus ground-truth depths for each of the six different sensor combinations are shown in Figure 9. There is excellent agreement between estimated and actual depths for the magnetometer, with 85% within 10 cm and 96% within 20 cm. The EM61 cart and MTADS-EM61 display a much larger scatter in actual and predicted depths — 74% and 76%, respectively, within 20 cm. For the EM61, the estimated depths of the deeper 4.2-inch mortars are particularly poor and contribute to the relatively wide range of estimated size observed for that class. The EM61 cart and MTADS-EM61 have a tendency to predict deeper depths for small, shallow items.

Cooperative inversion considerably improves the accuracy of the estimated depths: 75% of MTADS-EM61 depths are within 10 cm compared to 53% when inverted without magnetometer depth constraints. The performance gain is from 75% to 87% within 10 cm when the EM63 data are cooperatively inverted.

DISCUSSION

At the Camp Sibert site, the objective was to discriminate potentially hazardous 4.2-inch mortars from nonhazardous shrapnel, range, and cultural debris. We have described the performance of six different discrimination techniques that use data from the MTADS magnetometer array, a Geonics EM61 cart, the MTADS-EM61 array, and the Geonics EM63. From the extracted feature vectors, sev-

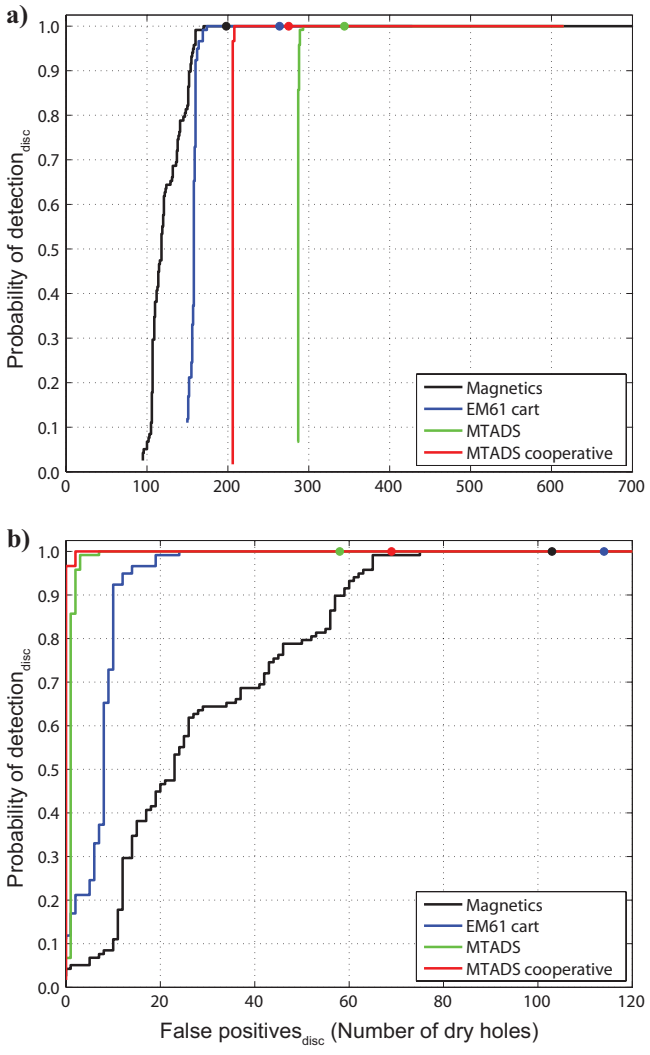

Figure 3. Comparision of ROC curves for the magnetics (moment), contractor EM61, MTADS-EM61, and MTADS-EM61 cooperative data sets: (a) including "can't analyze" category; (b) excluding "can't analyze" anomalies. The values for probability of detection and false positives are discriminatory (disc).

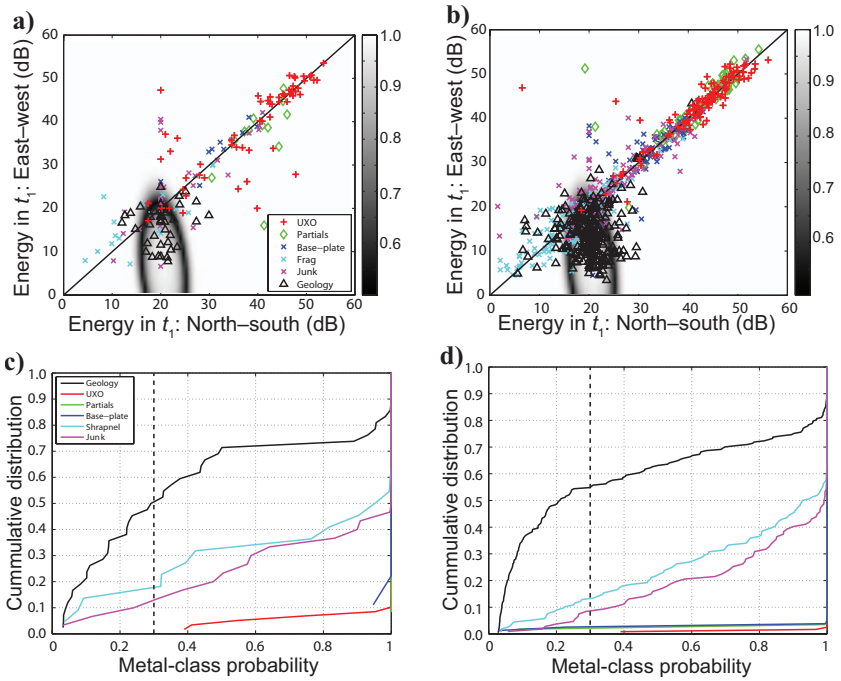

Figure 4. Reduction in geologic false alarms in the MTADS-EM61 data using the difference in the energy in the north-south versus east-west lines. (a) Training-data feature vectors (energy inside mask) overlying classifier decision surface. (b) The same as (a) but for test data. (c) Cumulative distributions on the training data for different categories when ranked by metal probability. (d) The same as (c) but for test data.

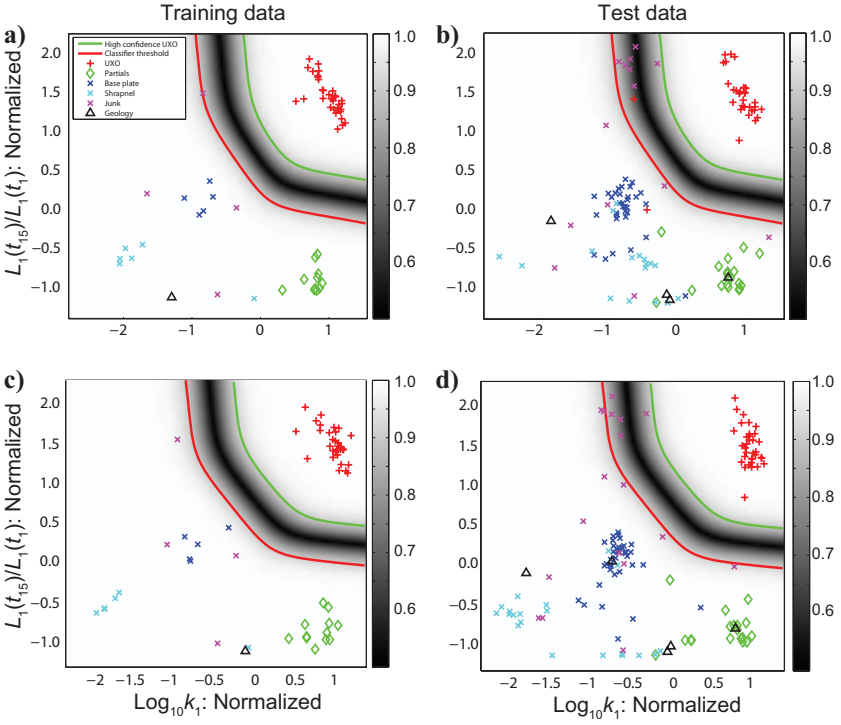

Figure 5. Feature vector plots for (a, b) the contractor EM63 and (c, d) the EM63 cooperative data sets. The plots on the left are for training data; those on the right are for test data.

en different prioritized dig lists were created: magnetics ranked by moment, magnetics ranked by remanence, EM61 statistical classification, MTADS-EM61 statistical classification, MTADS-EM61 cooperative inversion and statistical classification, EM63 statistical classification, and EM63 cooperative inversion and statistical classification.

In the blind-test data set, 119 seeded 4.2-inch mortars were left. Each of the seven methods successfully discriminated the mortars from nonhazardous items. For magnetics, the ranking by moment was better than that of remanence because of relatively large remanent magnetization of several of the seeded items. At the selected operating point, 76% of nonhazardous items were left in the ground and all mortars were recovered. Statistical classification of the contractor-collected EM61 data resulted in recovering all 4.2-inch mortars, with 59% of nonhazardous items left in the ground. For the MTADS-EM61 and MTADS-EM61 cooperative processes, all mortars were recovered, with 52% and 72%, respectively, of nonhazardous items unexcavated. The MTADS-EM61 results were degraded by the many "can't analyze" anomalies that had to be excavated as suspected UXO. Most of these were geologic artifacts caused by cart bounce as the MTADS-EM61 array traversed perpendicular furrows in a recently plowed field. Retrospective analysis revealed that many of these "can't analyze" anomalies could have been eliminated using an FOM or a geologic prescreener. The prescreener was based on a statistical classification of feature vectors related to the energy in the first time channel in the east-west versus north-south transects of the MTADS-EM61 array. More than 55% of the geologic anomalies could be rejected because they had significantly more energy north-south (perpendicular to the furrows) than east-west (parallel to the furrows).

By excluding the "can't analyze" category, we revealed the excellent intrinsic discrimination ability of the EM methods, particularly the MTADS-EM61 cooperative inversion. All 119 mortars were recovered with just three false positives, compared to 75, 25, and 8 false positives for the magnetometer, EM61, and MTADS-EM61, respectively. Stop-digging points were very conservative, with 103, 115, 59, and 70 false positives for the magnetometer, EM61, MTADS-EM61, and MTADS-EM61 cooperative, respectively.

The EM63 was deployed in a cued-interrogation mode over a subset of anomalies; the blind-test data comprised 150 items that contained 34 UXO. At the selected operating point, the EM63 statistical classification required 38 false positives, but one 4.2-inch mortar was missed. The failure was caused by a corrupt line of data that re-

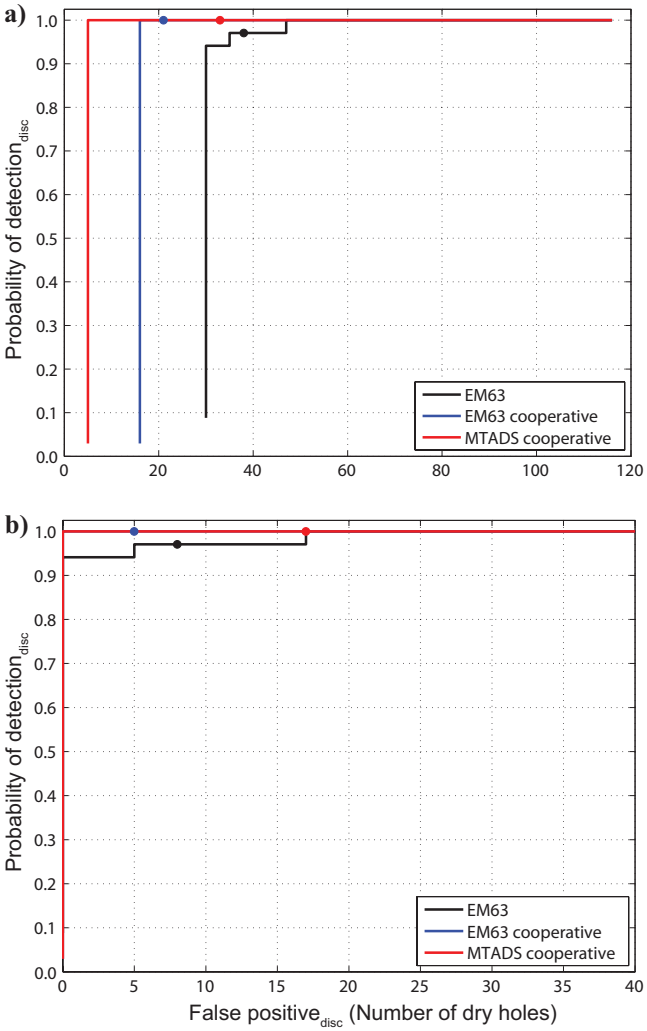

Figure 6. Comparision of ROC curves for the EM63 and EM63 cooperative data sets: (a) including the "can't analyze" category; (b) excluding the "can't analyze" anomalies. MTADS-EM61 cooperative results are also shown for comparison. The values for probability of detection and false positives are discriminatory (disc).

sulted in a small, shallow solution with a lower misfit than an alternative second solution closer to the true depth of burial. When the depth from the magnetometer was used as a constraint in the cooperative inversion process, the false negative did not occur. In fact, the EM63 cooperative produced a perfect ROC curve, with all 34 UXO recovered with zero false alarms. At the selected operating point, 21 false positives were required, with 16 of these in the "can't analyze" category.

The depth predictions of the magnetometer data are very accurate, with more than 85% within 10 cm and 96% within 20 cm of the true depths. The EM61 and MTADS-EM61 display a much larger scatter in actual and predicted depths, with 74% and 76%, respectively, within 20 cm. For the EM61, the estimated depths of the deeper 4.2 -inch mortars are particularly poor and contribute to the relatively wide range of estimated size observed for that class. The EM61 and MTADS-EM61 tend to predict deeper depths for small, shallow items.

Cooperative inversion considerably improves the accuracy of the estimated depths: 75% of MTADS-EM61 depths are within 10 cm, compared to 53% when inverted without magnetometer depth constraints. The performance gain is 75%–87% within 10 cm when the EM63 data are cooperatively inverted. The better-constrained depths of the cooperatively inverted EM models result in less scatter in the polarizabilities and improved discrimination ability.

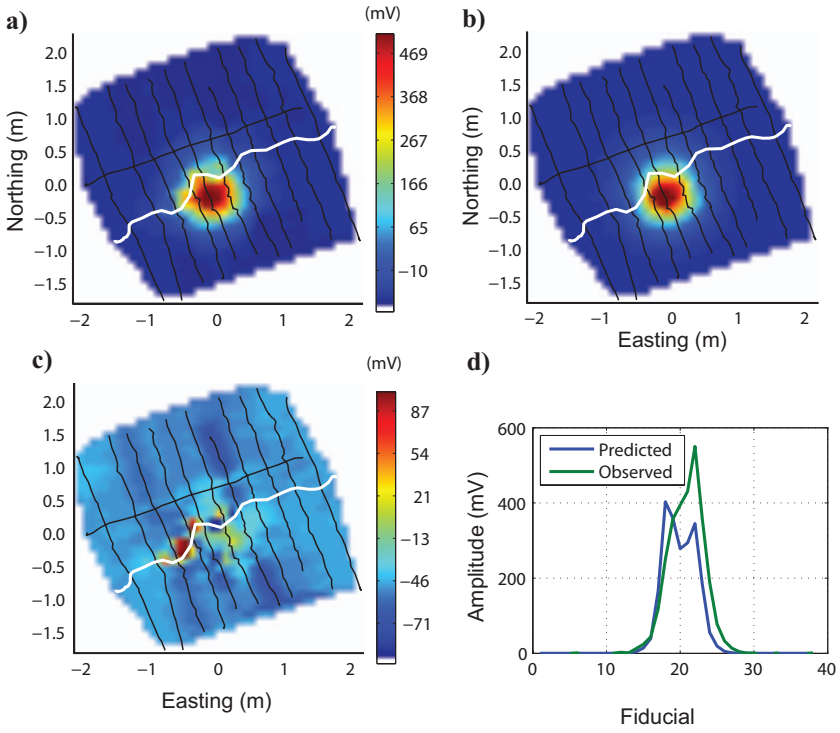

Figure 7. (a) Data, (b) model, and (c) residual of the first time-channel dipole model fit to anomaly 649 in the EM63 data. (d) Profile of the actual and fitted data in time channel 1 along the white line in views (a)–(c).

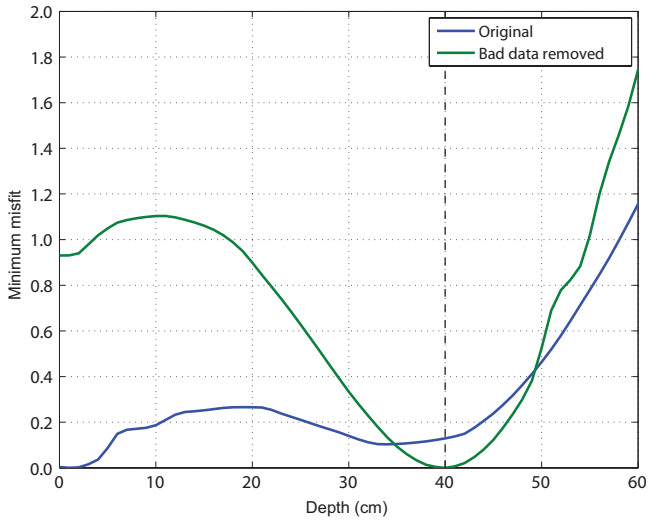

Figure 8. Misfit versus depth curve for the EM63 Pasion-Oldenburg model fit to anomaly 649. Two cases are considered: using all data that produce a shallow minimum close to the surface and after removing a "bad" line of data wherein the minimum occurs very close to the true depth of 40 cm (black dashed line).

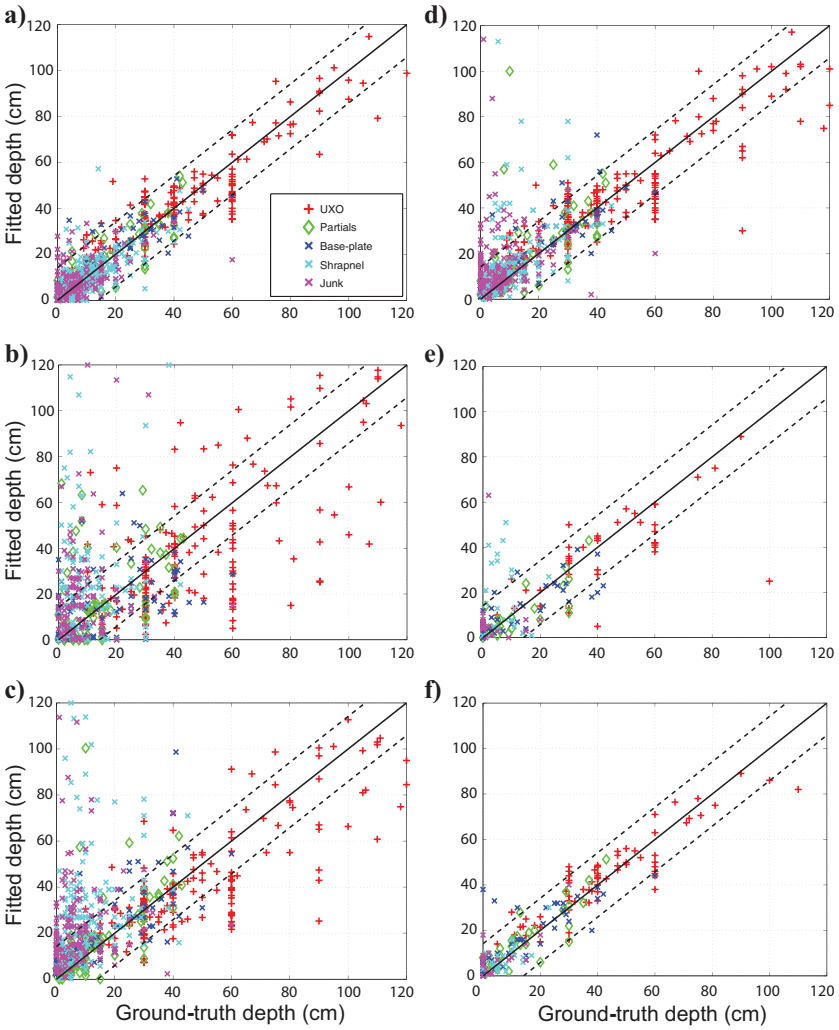

Figure 9. Scatter plot of fitted versus ground-truth depths for (a) magnetometer, (b) EM61, (c) MTADS-EM61, (d) MTADS-EM61 cooperative, (e) EM63, and (f) EM63 cooperative. The dashed lines represent errors of ±15 cm.

CONCLUSION

It is feasible to use magnetic and EMI data to reduce the number of nonhazardous items requiring excavation when attempting to clear a site contaminated with unexploded 4.2-inch mortars. The much richer information content of the EMI data sets compared to magnetometry results in better intrinsic discrimination performance, although some of the EMI data sets suffer from many "can't analyze" anomalies. Many of these were geologic artifacts caused by cart bounce as the sensor system traversed across furrows in a plowed field. Discrimination performance improved significantly when the depths of the EMI polarization models were constrained using magnetometry and/or as EMI data quality and information content increased (denser coverage, longer decay time measured, more accurate positions).

REFERENCES

Bell, T. H., B. J. Barrow, and J. T. Miller, 2001, Subsurface discrimination using electromagnetic induction sensor: IEEE Transactions on Geoscience and Remote Sensing, **39**, 1286–1293.

Beran, L., and D. W. Oldenburg, 2008, Selecting a discrimination algorithm for unexploded ordnance remediation: IEEE Transactions on Geoscience and Remote Sensing, **46**, 2547–2557.

Billings, S. D., 2004, Discrimination and classification of buried unexploded ordnance using magnetometry: IEEE Transactions on Geoscience and Remote Sensing, **42**, 1241–1251.

Billings, S. D., L. R. Pasion, and D. W. Oldenburg, 2002, Discrimination and identification of UXO by geophysical inversion of total-field magnetic data: U. S. Army Engineer Research and Development Center Report ERDC/GSL TR-02-16, http://el.erdc.usace.army.mil/uxo/pdfs/trg02-17.pdf, accessed 14 February 2010.

Bosnar, M., 2001, Geonics Ltd. Techical Note TN-33, http://geonics.com/pdfs/technicalnotes/tn33.pdf, accessed 14 February 2010.

Branch, M. A., T. F. Coleman, and Y. Li, 1999, A subspace, interior, and conjugate gradient method for large-scale bound-constrained minimization problems: SIAM Journal of Scientific Computation, **21**, no. 1, 1–23.

Collins, L., Y. Zhang, J. Li, H. Wang, L. Carin, S. Hart, S. Rose-Pehrsson, H. Nelson, and J. R. McDonald, 2001, A comparison of the performance of statistical and fuzzy algorithms for unexploded ordnance detection: IEEE Transactions on Fuzzy Systems, **9**, 17–30.

Das, Y., J. E. McFee, J. Toews, and G. C. Stuart, 1990, Analysis of an electromagnetic induction detector for real-time location of buried objects: IEEE Transactions on Geoscience and Remote Sensing, **28**, 278–287.

Gasperikova, E., T. J. Smith, H. F. Morrison, A. Becker, and K. Kappler, 2009, UXO detection and identification based on intrinsic target polarizabilities — A case history: Geophysics, **74**, no. 1, B1–B8.

Hart, S. J., R. E. Shaffer, S. L. Rose-Pehrsson, and J. R. McDonald, 2001, Using physics based modeler outputs to train probabilistic neural networks for unexploded ordnance classification in magnetometry surveys: IEEE Transactions on Geoscience and Remote Sensing, **39**, 797–804.

Lhomme, N., D. W. Oldenburg, L. R. Pasion, D. B. Sinex, and S. D. Billings, 2008, Assessing the quality of electromagnetic data for the discrimination of UXO using figures of merit: Journal of Engineering and Environmental Geophysics, **13**, 165–176.

McNeil, J. D., and M. Bosnar, 2000, Geonics Ltd. Technical Note TN-32, http://geonics.com/pdfs/technicalnotes/tn32.pdf, accessed 14 February 2010.

Nelson, H. H., T. H. Bell, J. R. McDonald, and B. Barrows, 2003, Advanced

MTADS classification for detection and discrimination of UXO: Environmental Security Technology Certification Program Final Report, http://www.estcp.org/viewfile.cfm?Doc-UX%2D4003%2DFR@sD01%2Epdf, accessed 14 February 2010.

Pasion, L. R., S. D. Billings, K. A. Kingdon, D. W. Oldenburg, N. Lhomme, and J. Jacobson, 2008, Cooperative inversion of time domain electromagnetic and magnetometer data for the discrimination of unexploded ordnance: Journal of Engineering and Environmental Geophysics, **13**, 193–210.

Pasion, L. R., and D. W. Oldenburg, 2001, A discrimination algorithm for UXO using time domain electromagnetics: Journal of Engineering and Environmental Geophysics, **6**, 91–102.

Smith, J. T., H. F. Morrison, and A. Becker, 2004, Parametric forms and the inductive response of a permeable conducting sphere: Journal of Environmental and Engineering Geophysics, **9**, 213–216.

Zhang, Y., L. M. Collins, and L. Carin, 2003a, Model-based statistical signal processing for UXO discrimination: Performance results from the JPG-V demonstration: 8th Conference on Detection and Remediation Technologies for Mines and Minelike Targets, SPIE, 5089, 1116–1126.

Zhang, Y., L. Collins, H. Yu, C. E. Baum, and L. Carin, 2003b, Sensing of unexploded ordnance with magnetometer and induction data: Theory and signal processing: IEEE Transactions on Geoscience and Remote Sensing, **41**, 1005–1015.